Current Sensorless Control for Single-Phase Boost-Type SMR

*Hung-Chi Chen (IEEE Member), **Chih-Kai Huang
*Department of Electrical and Control Engineering,
National Chiao Tung University, HsinChu, Taiwan.
**Industrial Technology Research Institute, HsinChu, Taiwan.

***Abstract*- In this paper, the single-loop current sensorless controls (SLCSC) for single-phase boost-type switching-mode-rectifiers (SMRs) are developed and digitally implemented in DSP-based system. Compared to the conventional multi-loop control with one inner current loop and one outer voltage loop, there is only one voltage loop in the proposed SLCSCs where its output is used to shift the nominal duty ratio pattern generated from the sensed input and output voltage. Because of no current loop, the efforts of sampling and tracking inductor current are unnecessary. It implies that the proposed SLCSCs are simple and very adaptable to the implementation with mixed-signal integrated circuits. It is also noted that the proposed SLCSCs are operated at continuous-current-mode (CCM). In this paper, first, the effects of shifting nominal duty ratio pattern on the input current waveform are analyzed and modeled with considering the inductor resistance and conduction voltages. It shows that the aligned current waveform can be inherently generated by the nominal duty ratio pattern and the current amplitude is roughly proportional to the shifting phase of nominal duty ratio pattern. Then, a voltage controller is included to regulate the dc output voltage by tuning this controllable phase. Finally, some simulated and experimental results have been given to demonstrate the performances of the proposed SLCSCs.**

I. INTRODUCTION

In DC/DC conversion, we often put close attentions on the performance of output voltage regulation. Alternatively, we are interested in the performances of input current shaping and output voltage regulation in the qualified AC/DC conversion. The use of switching-mode-rectifier (SMR) [1-3] with PFC function is an effective mean to perform the qualified AC/DC conversion. Boost-type SMRs as shown in Fig. 1 are the most popular circuit topology among all the others to shape the current waveform for their continuous current in the boost inductors.

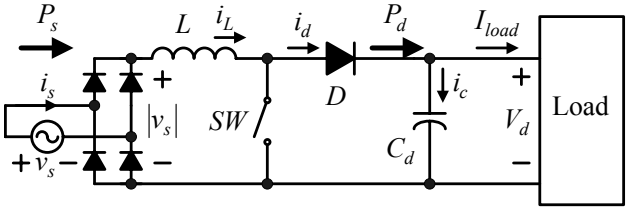

Fig. 1. Power circuit of the boost-type SMR.

Since there is only one controllable power switch in the boost-type SMR, both desired functions including input current shaping and output voltage regulation must be met by adequately turning on and turning off the single switch. In the conventional multi-loop control as shown in Fig. 2, the inner current loop and the outer voltage loop work together to achieve both desired functions by controlling the single switch where the former loop focuses on input current shaping and the latter loop contributes to voltage regulation, respectively.

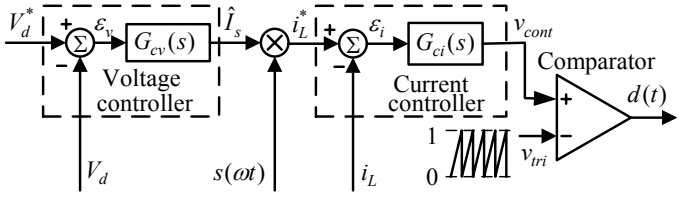

Fig. 2. Conventional multi-loop control for boost-type SMRs in CCM.

In order to perform the conventional multi-loop control, we need to sense three signals including input voltage, output voltage and input current. It is noted that the current sampling rate set according to the switching frequency is considerably greater than the voltage sampling rate decided based on the input line frequency. For single-phase boost-type SMRs, many voltage sensorless controls [4-5,7-9] and current sensorless controls [6-7] had been proposed in literatures in order to reduce the total number of input signals.

From the view of control structure, those sensorless control methods can be divided into two categories: one is multi-loop sensorless control and the other is single-loop sensorless control. Since there is only one voltage loop in the latter category, they can be seen as voltage-mode control and therefore, the former category can be regarded as current-mode sensorless control for their inner current loop.

In the boost-type SMR, the rising rate of current is proportional to the input voltage and the falling rate is proportional to voltage difference between the output voltage and input voltage. The above relations are used in the multi-loop sensorless control methods [4-6]. The input voltage in [4] is reconstructed from the rising rate of inductor current. The output voltages in [4-5] are estimated from the falling rate of the available inductor current. In [6], the current is predicted from duty ratio, the sensed input and output voltage.

It is noted that at least two current samplings within the durations of rising current or falling current must be obtained in order to calculate the time rate of change of current in [4-5]. In the multi-loop current sensorless control in [6], the actual voltage sampling frequency must be increased to the level of switching frequency to predict the current accurately [6]. It implies that the actual sensing effort does not decrease but increase as the developed sensorless method [4-6]. Because that the conventional multi-loop control structures are still used in [4-6], in fact, the complexities of the sensorless control

978-1-4244-1874-9/08/$25.00 ©2008 IEEE

methods increase. In addition, the value accuracy of inductance has a great effect upon the performances of multi-loop sensorless control in [4-6] for that they are based on the inductive relation between the inductor current and inductor voltage

The control techniques in [7-9] are the group of single-loop sensorless controls. Compared to multi-loop sensorless control in [4-6], the performance of the single-loop control is not sensitive to value accuracy of circuit elements since no circuit parameter is used in the control loop [7-9].

The commonly used voltage-mode PFC control illustrated in Fig. 3 can be seen as the first single-loop sensorless control without sensing input voltage and current where the single switch is directly controlled by the comparison of the output of the voltage loop and the triangle signal [7]. Though the discontinuous current is rich in harmonics and is far from the pure sinusoidal waveform, the simple control in Fig. 3 is able to meet some standards and it is usually used in many low-power applications.

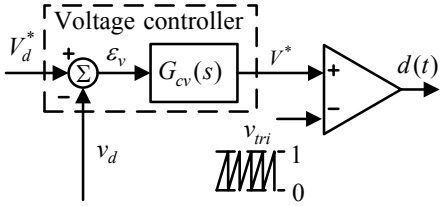

Fig. 3. Conventional voltage mode control for boost-type SMRs in DCM.

Both the nonlinear carrier control in [8] and the average current mode control in [9] are the other single-loop sensorlesss controls without sensing input voltage. The amplitudes of the nonlinear carrier signal [8] and the triangle carrier signal [9] are adjusted by the output of the single voltage loop. Then, their switching signals are generated from the result of comparison between the sensing current and the adjustable carrier signal. However, although there is no current loop in [8-9], the currents are sensed and the SMRs are operating under CCM, not under DCM. In this paper, the author develops the single-loop current sensorless control (SLCSC) without sensing any current. Like the other single-loop voltage sensorless control methods in [8-9], the SMRs with the proposed SLCSC also operate in CCM.

The paper is organized as follows. Initially, the effect of phase of the control signal on input current is analyzed and modeled. The results show that the sinusoidal current waveform can be automatically generated by the control signal and the input current amplitude is roughly proportional to the adjustable phase. Subsequently, based on the effect of phase on the input current amplitude, the voltage loop is included in SLCSC to regulate the dc output voltage by means of tuning the phase. Finally, some simulated and experimental results have been given to illustrate the performances of the proposed SLCSC.

II. BOOST-TYPE SMR

As shown in Fig. 1, the power circuit of the boost-type SMR mainly consists of a diode bridge rectifier and a boost-type DC/DC converter. From its circuit topology in Fig. 1, we can find that when input voltage v_s is positive, inductor current i_L is equal to input current i_s and that inductor current i_L is equal to minus input current $-i_s$ when input voltage v_s turns to negative. Then, the inductor current can be represented in terms of input current [10]

$$i_L(t) = sign(v_s(t))i_s(t) \tag{1}$$

where $sign(\bullet)$ is the sign operator and

$$sign(X) = \begin{cases} +1, when\ X \geq 0 \\ -1, when\ X < 0 \end{cases} \tag{2}$$

In order to model the behaviors of the boost-type SMR, some assumptions are initially made:

(i) Power switch *SW* is assumed to operate at a switching frequency approaching infinity. Thus, the input voltage over one switching period can be seen as constant.

(ii) A bulk capacitor C_d is included in the power circuit and thus, the output voltage can be assumed to be its average value V_d.

(iii) Without loss of generality, the input voltage is assumed to be $v_s(t) = \hat{V}_s \sin(\omega t)$ where $\hat{V}_s$ is the magnitude of input voltage.

(iv) When the boost-type SMR is operating in CCM with unity power factor, the input current can be assumed to be $i_s(t) = \hat{I}_s \sin(\omega t)$, where $\hat{I}_s$ is the magnitude of input current.

Therefore, the drawn input power $P_s(t)$ can be expressed as the product of input current $i_s(t) = \hat{I}_s \sin(\omega t)$ and input voltage $v_s(t) = \hat{V}_s \sin(\omega t)$.

$$P_s(t) = \frac{\hat{V}_s \hat{I}_s}{2} - \frac{\hat{V}_s \hat{I}_s}{2}\cos(2\omega t) \tag{3}$$

For the balance between input and output power, we are able to adjust the magnitude of sinusoidal current $\hat{I}_s$ to vary the output power in order to regulate output voltage. In the conventional multi-loop control as shown in Fig. 2, the magnitude $\hat{I}_s$ of sinusoidal current is tuned through the outer voltage loop. In the proposed SLCSCs, we can find that the magnitude $\hat{I}_s$ of sinusoidal current can be directly adjusted by the voltage loop without sensing any current.

III. Single-Loop Current Sensorless Control

The configuration of the proposed SLCSC with only one voltage loop is plotted in Fig. 4. Like the conventional controls plotted in Fig. 2 and Fig. 3, the duty signal $d(t)$ of SLCSC is also generated from the comparison between the fixed triangle signal v_{tri} and the control signal v_{cont}. However, it is noted that the control signal v_{cont} of SLCSC is at (-) terminal, and the fixed triangle signal v_{tri} is at (+) terminal. Besides,

compared with the current magnitude $\hat{I}_s$ at the output of voltage controller in Fig. 2, the output of voltage controller in proposed SLCSC is the controllable phase θ.

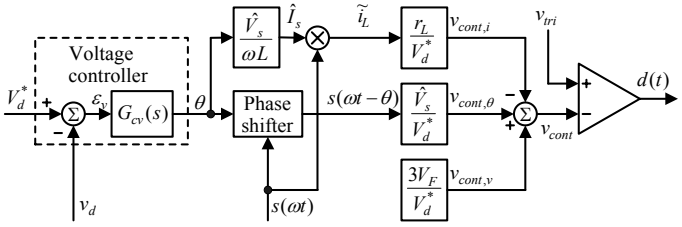

Fig. 4. Proposed SLCSC for boost-type SMRs.

The control signal v_{cont} in SLCSC composes of three signals and can be expressed as:

$$v_{cont} = v_{cont,\theta} - v_{cont,i} - v_{cont,v} \tag{4}$$

where

$$v_{cont,\theta} = \frac{\hat{V}_s}{V_d^*} s(\omega t - \theta) \tag{5}$$

$$v_{cont,i} = \theta \frac{\hat{V}_s}{\omega L} \frac{r_L}{V_d^*} s(\omega t) \tag{6}$$

$$v_{cont,v} = \frac{3V_F}{V_d^*} \tag{7}$$

and the signal $s(\omega t)$ denotes the unity rectified signal of input voltage $s(\omega t) = v_s(t)/\hat{V}_s$. In addition, r_L and V_F are the inductor resistance and diode/switch conduction voltage, respectively.

By combining the main circuit topology in Fig. 1 and the proposed SLCSC in Fig. 4, we can obtain the equivalent circuit model in Fig. 5 for simplified analysis where the diode rectifier is replaced by two series-connected diodes *DB*1 and *DB*2 and the input voltage is the ideal rectified sinusoidal voltage $\hat{V}_s|\sin(\omega t)|$. Then, the unity rectified signal $s(\omega t)$ is $s(\omega t) = |\sin(\omega t)|$ and $sign(v_s(t)) = sign(\sin(\omega t))$. In addition, in order to simply the following analysis, all the conduction voltages of the three diodes and the single switch *SW* are assumed equal to each other and denoted by V_F.

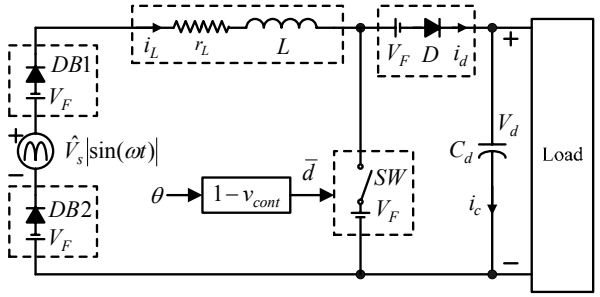

Fig. 5. Boost-type SMR with adjustable phase signal θ.

From Fig.4, since the control signal v_{cont} is at "-" terminal and the triangle signal v_{tri} is at "+" terminal, the average duty ratio signal $\bar{d}$ over one switching period can be expressed as:

$$\bar{d} = 1 - v_{cont} \tag{8}$$

From (4) through (8), the average duty ratio signal $\bar{d}$ can be further expressed in term of phase signal θ of voltage controller:

$$\bar{d} = 1 - \frac{\hat{V}_s}{V_d}|\sin(\omega t - \theta)| + \theta \frac{\hat{V}_s}{\omega L} \frac{r_L}{V_d}|\sin(\omega t)| + \frac{3V_F}{V_d} \tag{9}$$

From Fig. 5, when *SW* is turning on, the current flows through *DB*1, *SW* and *DB*2. Thus, the sum of total conduction voltage drops is $3V_F$. Otherwise, when *SW* is turning off, the sum of total conduction voltages is also $3V_F$ because that the current flows through *DB*1, *D* and *DB2*. Then, the following two KVL equations according to the conduction states of power switch *SW*.

$$L\frac{di_L}{dt} = \hat{V}_s|\sin(\omega t)| - 3V_F - i_L r_L \quad \text{when } SW \text{ is "on"} \tag{10}$$

$$L\frac{di_L}{dt} = \hat{V}_s|\sin(\omega t)| - V_d^* - 3V_F - i_L r_L \quad \text{when } SW \text{ is "off"} \tag{11}$$

Based on the time-averaging approach, the above two KVL equations can be combined to obtain (12) through multiplying them by turning-on time $\bar{d}T_s$ and turning-off time $(1-\bar{d})T_s$, respectively.

$$L\frac{d\,i_L(t)}{dt} = \hat{V}_s|\sin(\omega t)| - (1-\bar{d})V_d^* - 3V_F - i_L(t)r_L \tag{12}$$

where T_s is the switching period. Therefore, by substituting the averaged duty ratio signal $\bar{d}$ in (8) into (12) and arranging the terms, we can obtain the following time differential equations for inductor current

$$L\frac{d\,i_L(t)}{dt} = \hat{V}_s|\sin(\omega t)| - \hat{V}_s|\sin(\omega t - \theta)| + (\frac{\hat{V}_s\theta}{\omega L}|\sin(\omega t)| - i_L(t))r_L \tag{13}$$

where the terms of V_F are cancelled out.

Then, the term $\sin(\omega t - \theta)$ can be extracted by applying the approximations $\sin\theta \approx \theta$ and $\cos\theta \approx 1$ if the phase signal θ in radians is small and near to zero ($\theta \approx 0$) and the following trigonometric identity $\sin(A-B) = \sin A\cos B - \sin B\cos A$ and. Then, (13) can be rewritten as:

$$\begin{aligned}\frac{d\,i_L(t)}{dt} \approx & \frac{\hat{V}_s|\sin(\omega t)|}{L} - \frac{\hat{V}_s|\sin(\omega t) - \theta\cos(\omega t)|}{L} \\ & + (\frac{\hat{V}_s\theta}{\omega L}|\sin(\omega t)| - i_L(t))\frac{r_L}{L}\end{aligned} \tag{14}$$

Since the inductor current is repetitive with double line frequency $2f_{in}$, the current differential equation (14) can be simplified by removing the absolute operators

$$\frac{d\,i_L(t)}{dt} \approx sign(\sin(\omega t))[\frac{\hat{V}_s\theta}{L}\cos(\omega t)] + (\frac{\hat{V}_s\theta}{\omega L}|\sin(\omega t)| - i_L(t))\frac{r_L}{L} \tag{15}$$

Then, by solving (15), we can obtain the inductor current $i_L(t)$

$$i_L(t) \approx \frac{\hat{V}_s \theta}{\omega L}\left|\sin(\omega t)\right| = sign(v_s(t))[\frac{\hat{V}_s \theta}{\omega L}\sin(\omega t)] \quad (16)$$

From (1), the input current $i_s(t)$ can be express as

$$i_s(t) \approx \frac{\hat{V}_s \theta}{\omega L}\sin(\omega t) = \hat{I}_s \sin(\omega t) \quad (17)$$

From (17), obviously, the sinusoidal input current i_s is inherently generated without sensing current and current loop and its current amplitude $\hat{I}_s = (\hat{V}_s \theta)/(\omega L)$ is proportional to the controllable phase θ. Additionally, the sinusoidal input current i_s is in phase with the input voltage v_s. Therefore, we can include a voltage controller $G_{cv}(s)$ in SLCSC to automatically adjust the phase signal θ to control input power and regulate the output voltage. It shows that the desired performances including current shaping and output voltage regulation can be met by using the proposed SLCSC.

From (16), the component $v_{cont,i}$ of control signal v_{cont} can be expressed as:

$$v_{cont,i} = -i_L \frac{r_L}{V_d} s(\omega t) \quad (18)$$

From (7) and (18), obviously, the components $v_{cont,i}$ and $v_{cont,v}$ of control signal v_{cont} are used to compensate the effects of inductor resistance r_L and conduction voltage V_F. It also implies that the component $v_{cont,\theta}$ mainly contributes to the generation of sinusoidal current.

IV. Simulated Results

In this section, we begin with a series of computer simulations to demonstrate the proposed SLCSC. Some nominal values and circuit elements are listed in Table I. The simple plus-integral (PI) controller is used as the voltage controller in the developed SLCSC to adjust the phase.

Table I. Simulated circuit parameters

Input line voltage (peak)	$\hat{V}_s = 155V$ ($110V_{rms}$)
Output voltage command	$V_d^* = 300V$
Input line frequency	$f = 50Hz$
Smoothing inductance	$L = 4.65mH$
Smoothing capacitance	$C_d = 560\mu F$
ESR of boost inductance	$r_L = 0.9\Omega$
Conduction voltage	$V_F = 0.7V$
Carrier frequency	$f_{tri} = 25kHz$

By using the proposed SLCSC, the simulated waveforms of $R_{load} = 200\Omega$ are shown in Fig. 6 where the control signals v_{cont}, $v_{cont,i}$ and $v_{cont,\theta}$ are also plotted. From the simulated current waveform, it is noted that the output voltage is well-regulated to the voltage command $V_d^* = 300V$ and the yielded input current now is in the same form of sine function as that of input voltage. Therefore, although no current is sensed in the proposed SLCSC, the input current is well shaped and the high input power quality is obtained.

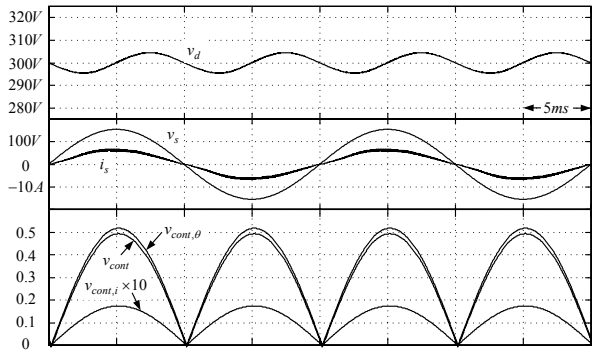

Fig. 6. Simulated waveforms of the proposed SLCSC under steady-state condition.

In order to understand the transient response of the proposed SLCSC, the simulated waveforms of sudden load change from $R_{load} = 200\Omega$ to $R_{load} = 177.78\Omega$ are shown in Fig. 7. From Fig. 7, the input current magnitude is increased from about 6.7A to about 7.3A by SLCSC in order to support sufficient power to regulate the output voltage to the desired one. We can also find that the sinusoidal current is in phase with the input voltage during the transient period. From the simulated waveform, it clearly shows that not only the output voltage regulation but also the input current shaping can be achieved by tuning phase signal θ in the proposed SLCSC.

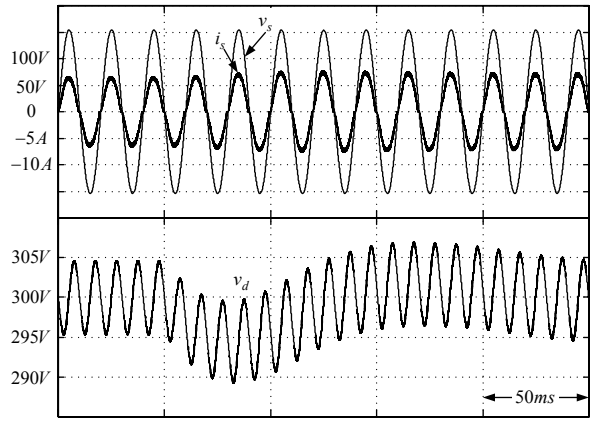

Fig. 7. Simulated waveforms of proposed SLCSC during load regulation.

V. Experimental Results

The proposed SLCSC has been digitally implemented in a DSP-based system using TMS320F240 where the simple PI-type voltage loop is used in order to focus on the performance of tuning the phase signal. Only input voltage and output voltages are sensed where the former provides the phase information of input voltage and the latter helps to regulate the output voltage.

It is noted that the digital resolution of duty phase is the main challenge in the implementation of the proposed SLCSC. Too small phase resolution would result in the instable

operation of SMRs in shaping current waveform. In the experiment, the digital resolution of phase signal θ is set to 0.00008π rads. For sinusoidal current waveform in SLCSC, the digital resolution of input current magnitude $\hat{I}_s$ and average input power are about $0.0267A$ and $2.075W$, respectively, corresponding to the digital resolution of phase signal θ. All the circuit parameters in the experimental system have been listed in Table I.

Fig. 8 shows the experimental waveforms for the proposed SLCSC at the condition $V^* = 300V$ and $R_{load} = 177.78\Omega$. The phase signal θ shown in the middle plot keeps around 0.021π rads in order to stably yield enough input power to regulate the output voltage. It is noted the phase signal $\theta \approx 0.021\pi$ is so small that it is reasonable to use the approximations $\sin\theta \approx \theta$ and $\cos\theta \approx 1$ in order to derive (14).

The average duty signal $\bar{d}$ is also plotted to show the variation of duty ratio. We can find that maximum duty ratio is 100% and minimum duty ratio is about 48% equal to the ratio of input voltage magnitude $\hat{V}_s = 155V$ and the output voltage $V_d = 300V$. From the bottom plots of input current i_s and input voltage v_s, the proposed SLCSC possesses good PFC function including input current shaping and output voltage regulation without sensing any current.

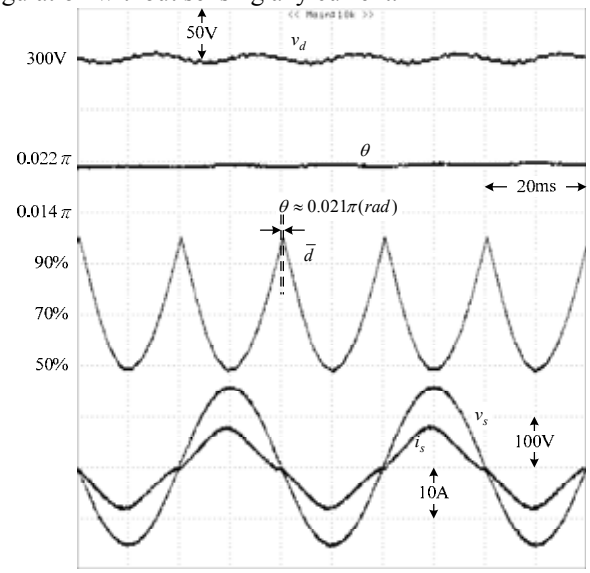

Fig. 8. Experimental waveforms with SLCSC.

To verify the dynamic performance of the proposed SLCSC, some experimental results are shown in Fig. 9 where the load resistance R_{Load} is suddenly changed from 200Ω to 177.78Ω. In order to regulate the out voltage, the phase signal θ tunes to increase due to PI-type voltage controller in order to yield sufficient input current and input power. During the regulation, the input current keeps in phase with the input voltage. It clearly shows that the proposed single-loop CSC also possesses good regulation ability.

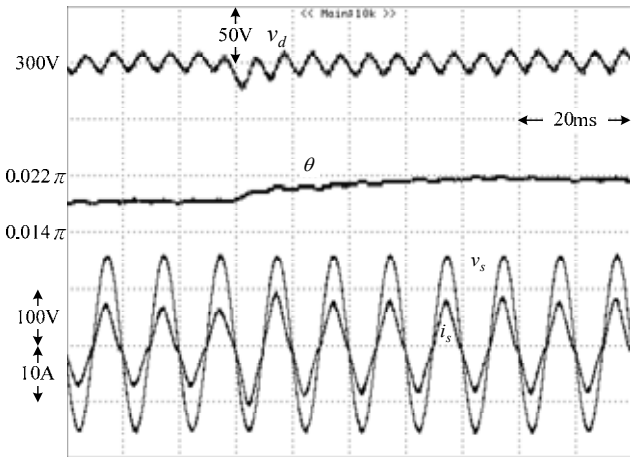

Fig. 9. Experimental waveforms with SLCSC during load regulation.

The input voltage and input current with various load resistances 300Ω, 400Ω and 500Ω are plotted in Fig. 10(a) and Fig. 10(b), respectively. Obviously, with large load resistance, the input currents tend to return to zero current early and be blocked to zero current until the next half line-cycle. Due to the stagnated current, the degraded quality including total current harmonic current (*THDi*) and power factor (*PF*) are plotted in Fig. 11(a) and Fig. 11(b), respectively. In other words, not only the limited resolution of phase θ but also the degraded quality, we can find that the proposed SLCSC is not suitable under light load.

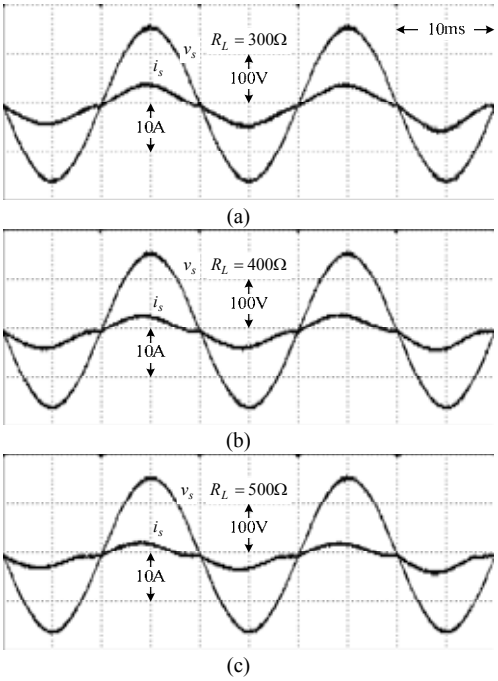

Fig. 10. Input voltage and input current with various load resistances: (a)300Ω; (b)400Ω; (c)500Ω.

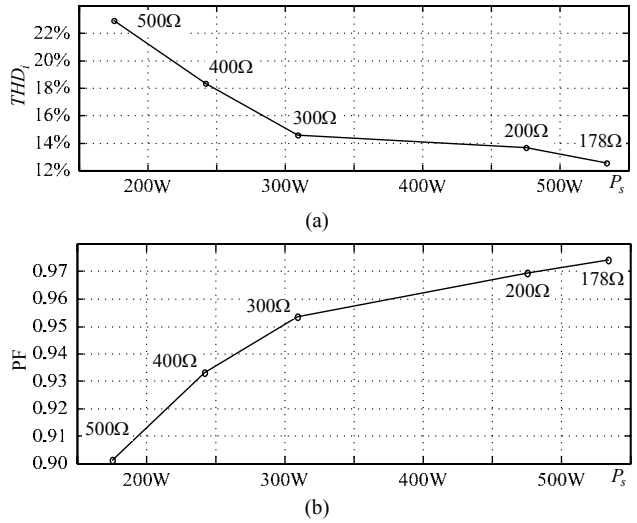

Fig. 11. (a) Total current harmonic distortion versus input power; (b) power factor versus input power.

VI. CONCLUSIONS

In this paper, a new SLCSC for boost-type SMR had been proposed. Compared to the conventional PFC control, the output of voltage loop is the phase signal used to shift the reference control signal. The proposed SLCSC had been developed and implemented in DSP-based system. The simulation and experimental results clearly demonstrate the proposed SLCSC. However, due to limited-bits resolution of phase signal and the degraded quality under light load, the application of the proposed SLCSC is not preferred to be used with the light load.

ACKNOWLEDGMENT

The author wish to thank the financial support under Grant NSC 96-2221-E-009-247 from the National Science Council in Taiwan.

REFERENCES

[1] O. Garcia, J. A. Cobos, R. Prieto, P. Alou, and J. Uceda, "Single phase Power Factor Correction: A Survey," *IEEE Trans. on Power Electronics*, vol. 18, no. 3, pp. 749-754, May 2003.

[2] H. C. Chen, S. H. Li, and C. M. Liaw, "Switch-Mode Rectifier with Digital Robust Ripple Compensation and Current Waveform Controls", *IEEE Trans. on Power Electronics*, vol. 19, no. 2, pp. 560-566, March 2004.

[3] M. Chen, and J. Sun, "Feedforward Current Control of Boost Single-Phase PFC Converters," *IEEE Trans. on Power Electronics*, vol. 21, no. 2, pp. 338-345, March 2006.

[4] S. C. Yip, D. Y. Qiu, H. S. Chung, and S. Y. R. Hui, "A Novel Voltage Sensorless Control Technique for a Bidirectional AC/DC Converter", *IEEE Trans. on Power Electronics*, vol. 18, no. 6, pp. 1346-1355, Nov. 2003.

[5] A. Pandey, B. Singh, and D. P. Kothari, "A Novel DC Bus Voltage Sensorless PFC Rectifier with Improved Voltage Dynamics," *in IEEE IECON'02*, pp. 226-228, 2002.

[6] S. Sivakumar, K. Natarajan, and R. Gudelewicz, "Control of Power Factor Correcting Boost Converter Without Instantaneous Measurement of Input Current," *IEEE Trans. on Power Electronics*, vol. 10, no. 4, pp. 435-445, Jul. 1995.

[7] D. S. L. Simonetti, J. L. F. Vieira and G. C. D. Sousa, "Modeling of the High-Power-Factor Discontinuous Boost Rectifier," *IEEE Trans. on Industrial Electronics*, vol. 46, no. 4, pp. 788-795, Aug. 1999.

[8] D. Maksimovic, Y. Jang, and R. W. Erickson, "Nonlinear-Carrier Control for High-Power-Factor Boost Rectifiers", *IEEE Trans. on Power Electronics*, vol. 11, no. 4, pp. 578-584, Jul. 1996.

[9] J. Rajagopalan, F. C. Lee, and P. Nora, "A General Technique for Derivation of Average Current Mode Control Laws for Single-Phase Power-Factor-Correction Circuits Without Input Voltage Sensing", *IEEE Trans. on Power Electronics*, vol. 14, no. 4, pp. 663-672, Jul. 1999.

[10] D. M. Van, K. D. Gusseme, A. P. M. V and J. A. Melkebeek, "Duty-Ratio Feedforward for Digitally Controlled Boost PFC Converters", *IEEE Trans. on Industrial Electronics*, vol. 52, no. 1, pp. 108-115, Jan. 2005.